Particle Accelerators
1980 Vol.10 pp.235-251
0031-2460/80/1003-0235$06.50/0

SPACE-CHARGE ION OPTICS INCLUDING EXTRACTION FROM A PLASMA

J. H. WHEALTON and J. C. WHITSON

Oak Ridge National Laboratory, Oak Ridge, Tennessee 37830 USA

(Received September 20, 1979)

The effect of source plasma properties and extraction electrode dimensions on ion-beam optics is examined theoretically using an algorithm for a solution to the Poisson-Vlasov equation with explicit consideration of the cylindrically symmetric two-dimensional collisionless sheath. Plasma electrons are assumed to have a Boltzmann distribution; the algorithm for the nonlinear Poisson equation has proven convergence and uniqueness properties. Ion optics as a function of source plasma density, electron temperature, fluctuations, and plasma potential are examined as well as the effect of electrode dimensions such as aspect ratio and thickness. The ion properties examined are beam divergence with relative contributions of aberrations, nonoptimum perveance, sensitivity to non-optimum conditions. Also considered is actual transmission including non-geometric electrode absorption.

I. INTRODUCTION

Recent evidence indicates the possibility that neutral-beam heating of toroidal plasmas is effective.[1-15] These neutral beams are formed from ion sources.[3,16-28c] In these ion sources, ions are extracted from a plasma, accelerated in an electrostatic field to the desired energy (20–200 kV), and traverse an electron-capture cell; this results in a substantial fraction of the ions becoming neutrals. These neutrals are able to go through the fields of magnetic-confinement devices and penetrate a substantial distance into the confined plasma. Various design considerations require the source to be far away (on the order of meters) from the aperture of the confinement device. This aperture, through which the beam must pass, is of dimensions such that it subtends an angle on the order of 1° from the source. The desire to pass a large fraction of the beam through an aperture of this solid angle puts considerable demands on the neutral-beam system in general and on the source plasma and ion extraction in particular. The optical properties of such ion beams extracted from a plasma are the subject of this paper.

Several types of plasma generators are currently used for neutral-beam sources. One such generator is the thermionic-cathode reflex discharge[29-35] followed by an expansion chamber.[3,12,16,18,21-28,36-46] Another generator is a magnetic field-free thermionic cathode with a high-current and low-pressure diffuse discharge.[8,19,20,26-28,47-56]

In order to form very high perveance beams, they are extracted from multiaperture electrodes with either cylindrical holes[3,17,18,23-28,36,37,40,41,43-45,57-81] or slots.[20,38,50-56,74-77,82-86]

Some penetration into the problem of the focusing of ions extracted from a plasma can be done from analysis of the paraxial equations coupled with a model for the sheath. Such an analysis has been done[71,67,87] using the paradigm that the sheath is like a spherical diode with space-charge limited flow.[88-90] This model is coupled to a solution of the paraxial equations for an aperture.[91,92] Extensions of this analysis to more specific systems, including space charge, are available.[66,81,93-106] This analysis has several defects as follows. The optimum beam convergence is limited only by the source-plasma ion temperature, whereas it is frequently limited by spherical aberrations[64,66-69,73] amplified by source-plasma fluctuations.[107] The predictions of optimum perveance do not take into account the plasma which hits the inside bore of the plasma electrode. This effect varies between 10%[64,67,73] and 50%.[64,66,67] A conceptual defect is that the ion flow has been claimed to be space-charge limited[3,18,19,23,70,76,77,85,86,108-117] rather than entirely emission limited.[64,118,119] This can be seen by noting that for ion extraction from a plasma, the electrons would fill the space-charge well formed by the ions as the space-charge limit was ap-

proached. This is in contrast to electron beams extracted from a surface where there is no copious supply of positive ions to fill the analogous space-charge well. The fact that important beam parameters are proportional to the ion current on the scale of the Child[88]-Langmuir[89] space-charge limited current is a reflection of the fact that the beam current is an important parameter, not that there is space-charge limited flow.

Machine computations are available using algorithms that iterate between a solution of Poisson's equation and a calculation of ion trajectories with deposition of space charge. The earliest efforts started the ions on a surface in the aperture on which the electric field was taken to be zero and through which source plasma electrons do not penetrate.[19,77,80,83,111,116,119–133] This is an approximation of dubious validity because there is no region of space where the electric field and the plasma electron density are both small.

An improvement in this early method included the space charge as a Boltzmann distribution and iterated the electron space charge along with the solution of the Poisson equation.[85,134,135] The ions are started off on an equipotential surface in the sheath region of the source plasma. The approximate position, potential, and field of this surface, as well as the initial directed ion speed, are given by a solution to the collisionless one-dimensional Poisson-Vlasov equation in the sheath region.[136] A procedure has been worked out that, given the emitting surface potential, adjusts the emitter position automatically so that the electric field is consistent with the one-dimensional solution. However, this presumes that the electric field is the same and is constant along such a potential surface in the actual two-dimensional problem; we will examine this conjecture later. Another problem is that the ion direction at the sheath must be specified even though it is unknown for the two-dimensional case. In typical cases the emitting surface is approximately 15 Debye lengths from the plasma electrode.[135] Presumably, if the emitting surface could be taken sufficiently far into the plasma, the problem becomes more one-dimensional and utilization of the one-dimensional sheath solution would be more reliable. Unfortunately, these iteration schemes[85,134,135] converge very slowly, if at all, for emitting positions far back (100 Debye lengths) into the plasma[68] (see the curve labeled A in Fig. 1).

Further improvements in the iteration scheme (see curves labeled B and C in Fig. 1) have enabled the emitter to be taken far back into the plasma, but the accuracy of the solutions could use improvement (e.g., see Ref. 64).

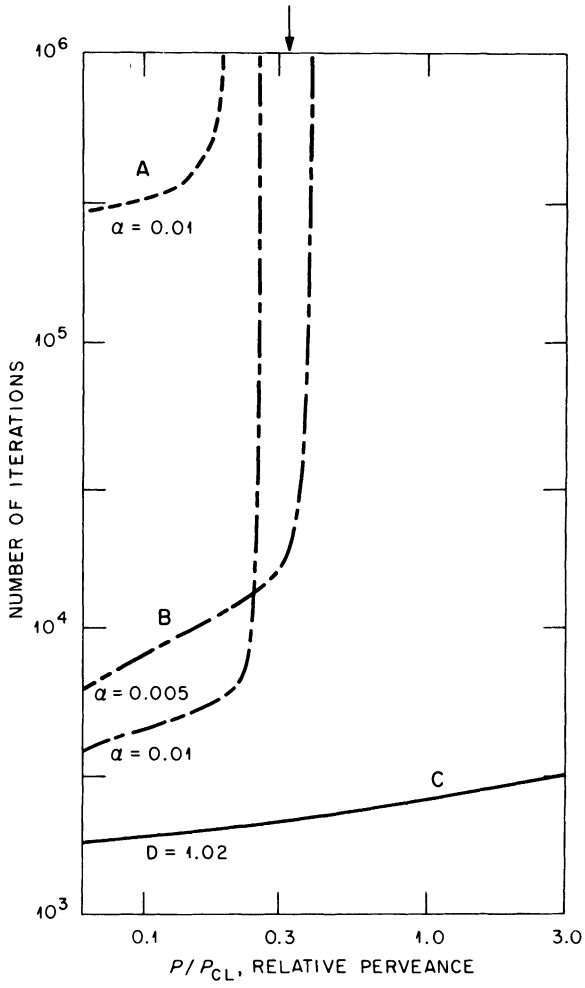

FIGURE 1 Expeditiousness of three different explicit iteration algorithms for the Poisson equation: A denotes sequential constant electron underrelaxation, B denotes simultaneous constant electron underrelaxation, and C denotes simultaneous accelerated electron underrelaxation. The expeditiousness is plotted as a function of the perveance on the scale of the Child-Langmuir perveance, over a range for part of which the former two schemes do not converge at all.

In Sec. II we describe the computational technique used herein which eliminates the difficulties in previous schemes.[68,85,134,135] In Sec. III we examine the effect of plasma properties on ion optics, emittance, transmission, and optimum perveance. In Sec. IV we examine the effect of electrode dimensions on the same quantities. In

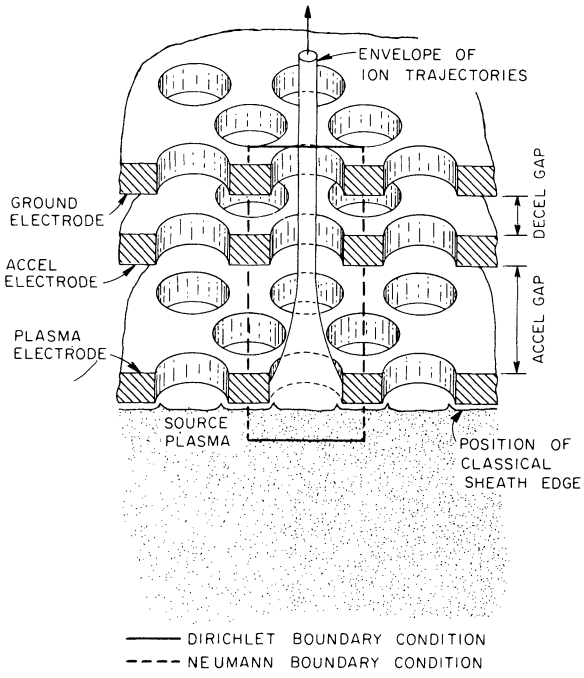

FIGURE 2 Diagram showing the region of consideration in the solution of the Poisson-Vlasov equation. Adjacent holes, beamlet and plasma are represented by cylindrically symmetric Neumann boundary conditions.

Sec. V we present conclusions and examine more explicitly the assumptions of previous work in terms of the results presented in Secs. III and IV.

II. MATHEMATICAL FORMULATION AND COMPUTATIONAL TECHNIQUE

We solve the Poisson equation,

$$\nabla^2\phi = \frac{e}{\epsilon_0}(N - n), \tag{1}$$

where the electron density N is assumed to be in equilibrium,

$$N = N_0 \exp[e(\phi_0 - \phi)/kT_e], \tag{2}$$

and N_0, T_e, and ϕ_0 are respectively the source plasma density, electron temperature, and potential. The ion density n in Eq. (1) is determined by a Vlasov equation for the distribution function,

$$\mathbf{v}\cdot\nabla f - \frac{e}{m}\nabla\phi\cdot\nabla_v f = 0, \tag{3}$$

which couples to Eq. (1) by

$$n = \int f\, d\mathbf{v}. \tag{4}$$

These equations have been solved previously.[68,69,85,134,135,137,138] The electron space charge [Eq. (2)] has in recent attempts[68,69,137,138–140] been inserted with sufficient accuracy and stability to allow a solution in the entire two-dimensional sheath. Therefore, initial data consist of the stipulation that the ions are only slightly perturbed from equilibrium on a surface that is chosen to be only slightly removed from the plasma potential. Typical boundary data are shown in Fig. 2 showing Dirichlet and Neumann boundary conditions.

Poisson's Eq. (1) and the electron source term are solved implicitly by a finite difference method on a mesh with given ion-source terms, by a Newton successive-overrelaxation method.[69,138,139,141] This method is very accurate, as shown in Fig. 3 compared with scheme C shown in Fig. 1. Boundaries are treated using a procedure developed by Hornsby.[142] Vlasov's Eq. (3) is solved indirectly by a solution of orbit equations by use of a deferred-limit integrator[133,139] and ion charge deposited on the mesh points in accordance with the continuity equation.

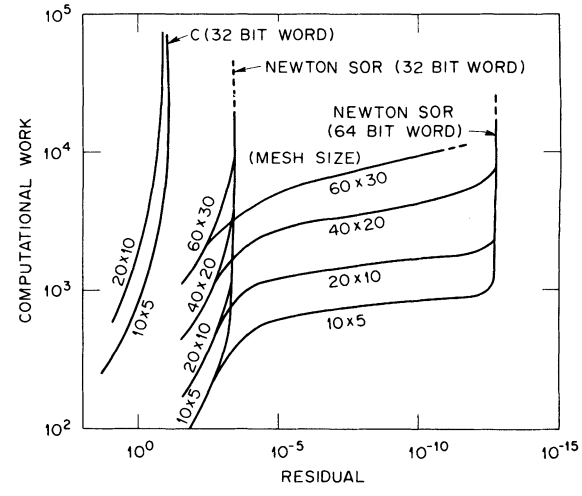

FIGURE 3 Expeditousness of two different algorithms for the Poisson equation: C denotes the simultaneous accelerated electron underrelaxation scheme, described in Fig. 1, and an implicit Newton SOR algorithm. All are shown as a function of mesh size, word size, and specified accuracy.

Shown in Fig. 4 are the following: (1) the effect of ion space charge on ion optics; (2) the position of the three electrodes, as illustrated in Fig. 2; and (3) equipotential contours. The leftmost equipotential contour is about halfway between the source plasma potential and the plasma electrode, which in this example is assumed isolated electrically. The remaining equipotential contours are at 5% intervals up to 95% of the maximum acceleration potential; for potentials greater than 95% the equipotentials are shown at 1% intervals. Shown in Fig. 4(a) are ion trajectories through the fields neglecting any ion space charge. The trajectories show a large divergence, the root-mean-square (rms) angle being about 10°. The ion space charge is inserted, and the Poisson equation is reiterated. Eventually, typically after seven such ion iterations, the result converges to a solution, which is shown in this example in Fig. 4(b). The leftmost equipotential contour has moved significantly from that in Fig. 4(a) and is illustrative of the position of the sheath edge. The second leftmost potential contour is also significantly shifted and illustrates the nature of the large radial fields near the plasma electrode. The ions are affected by these fields a great deal since they are moved so slowly in this region. The rms angle in Fig. 4(b) is about 2.5°, which is significantly less than that of Fig. 4(a), but much greater than that expected from the initial ion thermal energy. The emitter position in Fig. 4 is taken to be 100 Debye lengths from the plasma electrode, and the plasma density in Fig. 4(b) is approximately optimum for minimum beam divergence. Also shown in Fig. 4(b) are ions from the source plasma that are outside the geometric shadow of the electrodes but which strike the inside surface of the plasma electrode aperture. This is a loss of transmission, which has the effect of lowering the arc efficiency of the source.

A more detailed view of the sheath region is shown in Fig. 5 for a case where the radius of the electrodes is twice that of Fig. 4. The source plasma density is optimized for minimum beam divergence, and the emitter position is taken at 100 Debye lengths from the plasma electrode.Two more equipotential contours have been added to this figure from that of Fig. 4 to show more explicitly the sheath thickness and radial aberration fields. As in Fig. 4 the leftmost potential contour is halfway between the source plasma and the plasma electrode. The second potential contour just to the right of this is approximately at the

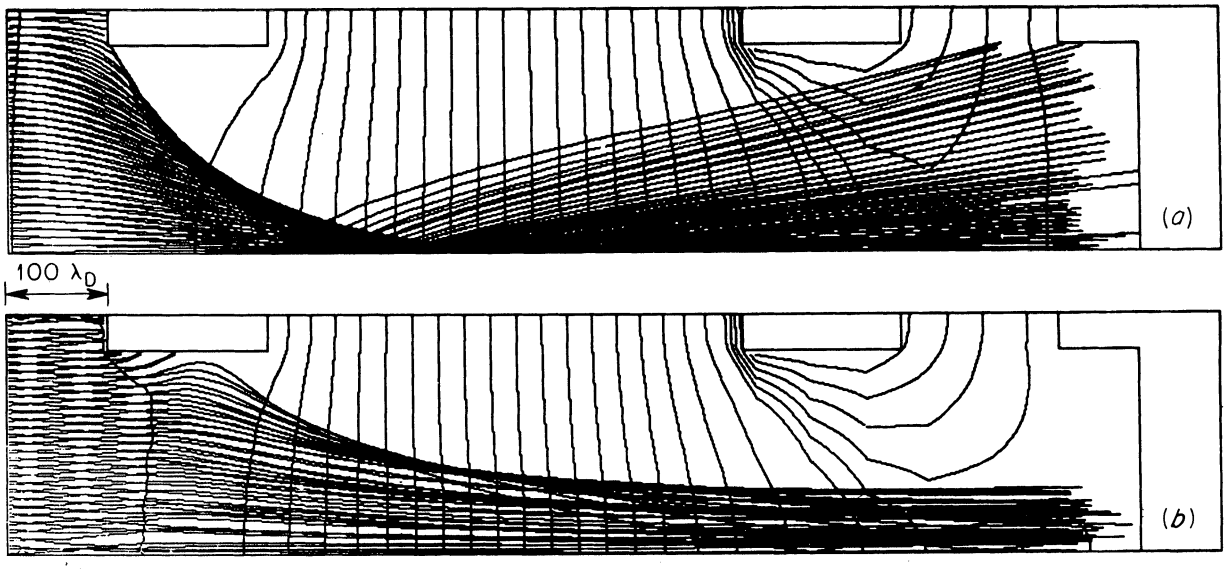

FIGURE 4 Equipotential contours, electrodes, and ion orbits for two cases: (a) vacuum and (b) converged solution including ion and electron space charge. The leftmost contour in case (b) shows the approximate location of the classical edge.

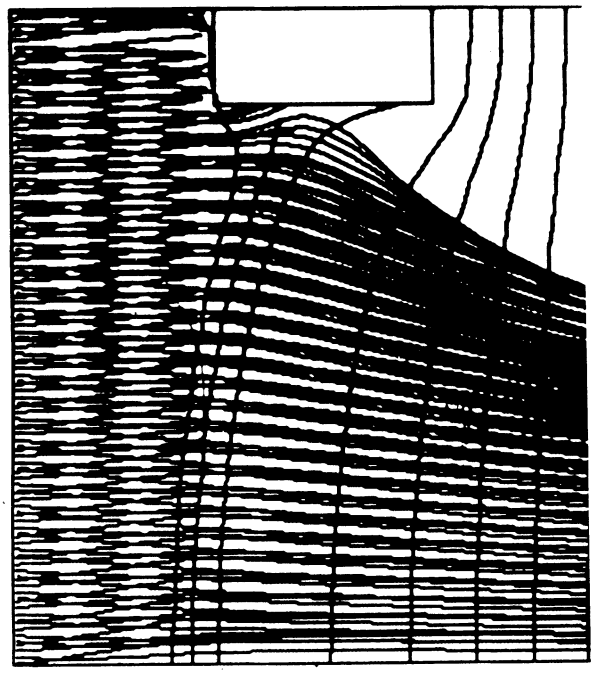

FIGURE 5 Equipotential contours, plasma electrode, and ion orbits for a converged solution in the region near the sheath.

plasma electrode potential. The third contour is at four times the difference between the source plasma and the plasma electrode. This case illustrated in Fig. 5 shows that the distance between the potential of the classical sheath edge and the potential of equal ion and electron flux is about 10 Debye lengths.

In most cases, as illustrated in Figs. 4 and 5, the ion optics at optimum source-plasma density is determined by aberrations near the plasma

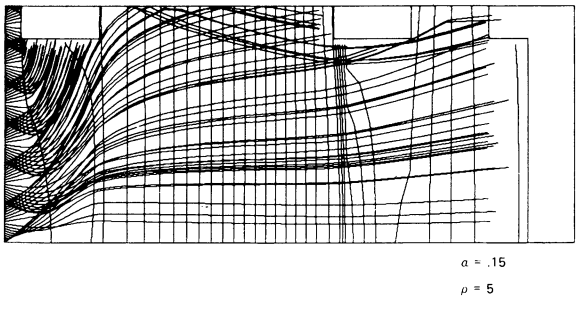

FIGURE 6 Equipotential contours, electrodes, and ion trajectories for a plasma density ten times that for minimum beam divergence. The aberration fields near the plasma electrode are seen to be negligible.

electrode. However, for sufficiently high plasma density the situation is different, as illustrated in Fig. 6. Here the plasma density is so large that the ion current density at the emitter is five times the Child-Langmuir space-charge limit. There are virtually no aberrations due to the first electrode and most of the beam divergence is due to non-optimal sheath shape. Note how the second electrode acts as a diverging lens, as predicted by the paraxial analysis. The effect of the Neumann boundary condition on the top surface reflects itself in ions entering the region from adjacent beamlets. The vertical magnification of Fig. 6 is a factor of 4 for easy viewability. Most phenomena governing ion optics are illustrated in Figs. 4–6. A detailed study follows.

From dimensional considerations[144,145] there are only three parameters that determine the ion optics for a fixed or similar geometry.[64] These parameters are $\beta_e \equiv e\phi_A/kT_e$, $\beta_i \equiv e\phi_A/kT_i$, and $\rho \equiv (9Nd^2/4\epsilon_0)(ekT_i/\pi\phi_A^3)^{1/2}$, where ϕ_A is the applied accelerating potential difference across a gap d and T_i is the source ion temperature. Thus, an examination of the effect on ion optics of the source plasma density, electron temperature, and ion temperature represents a complete parameter study for fixed or similar geometry electrodes. This is the subject of Sec. III.

III. EFFECT OF PLASMA PROPERTIES ON ION OPTICS

A. *Plasma Density*

The effect of plasma density on ion trajectories is shown in Fig. 7 for three values of the plasma density parameter ρ. As is well known, there is an optimum plasma density for minimum beam divergence. For the geometry shown in Fig. 7 (which is magnified by a factor of 2 in the radial direction for easy viewability) this optimum perveance is at $\rho \cong 0.4$, shown in Fig. 7(b). For a density significantly below this (e.g., $\rho = 0.2$), shown in Fig. 7(a), the beamlet is very narrow but has very large wings in the distribution. This is seen more explicitly in Figs. 8–10, which show emittance diagrams for the three cases shown in Figs. 7(a–c), respectively. In these emittance diagrams the slope dr/dz of each trajectory and its radial position are denoted. To make it look like conventional Cartesian emittance diagrams, the points are reflected through the position origin. For an under-dense plasma, as shown in Fig.

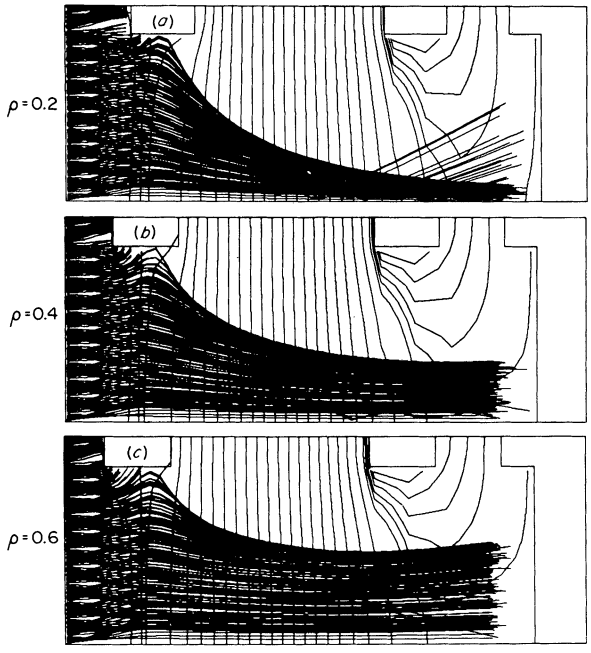

FIGURE 7 Equipotential contours, electrodes, and ion trajectories for three cases of differing source plasma density.

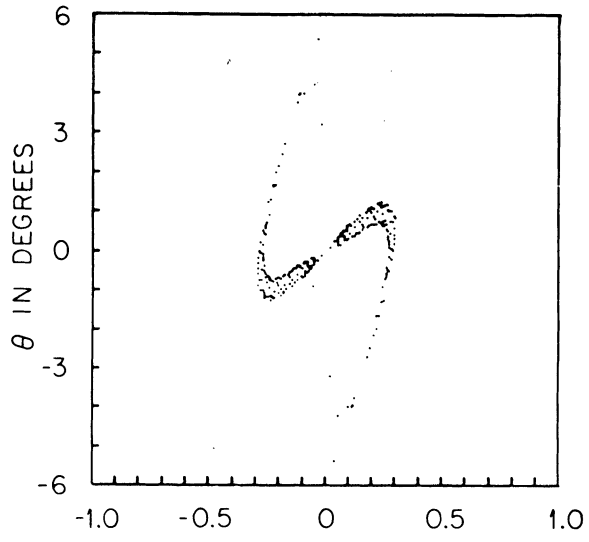

FIGURE 9 Emittance diagram for the case (ρ = 0.4) shown in Fig. 7(b).

8 (compared to Fig. 9), the wings of the beamlet angular distribution are relatively large. In contrast, for an over-dense plasma [shown in Figs. 7(c) and 10 for ρ = 0.6], the entire distribution has a relatively large divergence compared to the ρ = 0.4 case, but the tails contribute a relatively minor amount. For this case the beam divergence may be made much smaller by insertion of converging electrostatic lens. This is the principle of operation of a tetrode ion accelerator.[66] No similar rectification of the large-divergence beam resulting in the under-dense case (ρ = 0.2) is feasible, because in this case there is not generally

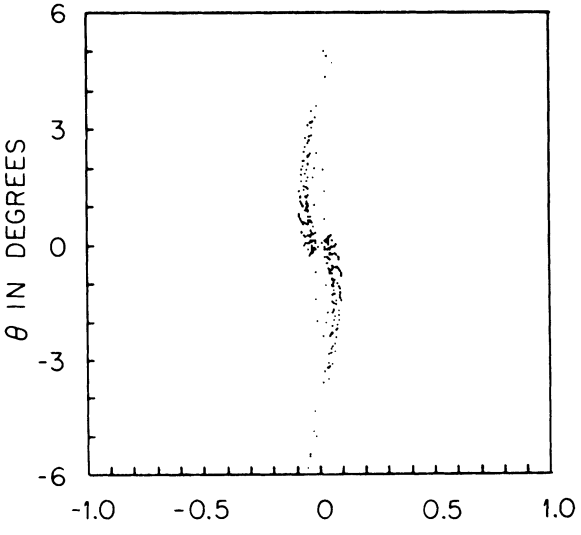

FIGURE 8 Emittance diagram for the case (ρ = 0.2) shown in Fig. 7(a).

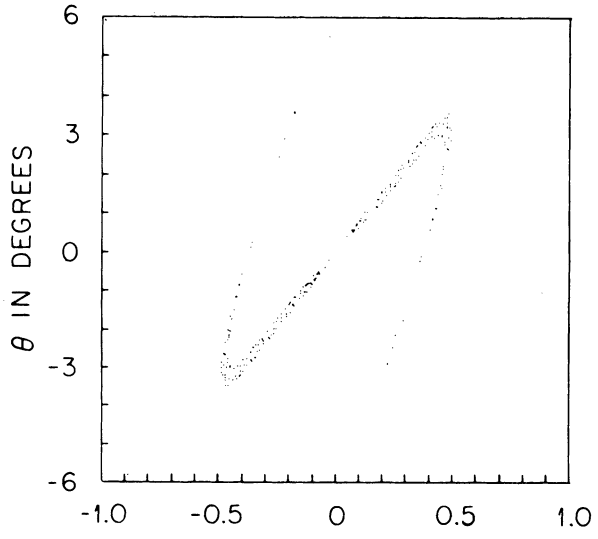

FIGURE 10 Emittance diagram for the case (ρ = 0.6) shown in Fig. 7(c).

a single-valued correlation of divergence and position. In other words, the large divergence in the over-dense case is due to linear space-charge blowup, whereas in the under-dense case it is principally due to nonlinear aberration fields. The $\rho = 0.4$ case shown in Figs. 7(b) and 9 is the optimum density for minimization of the rms angle of the trajectories. However, for profile measurements[66,67,73] which are done with high accuracy only near the center of the distribution, the apparent optimum plasma density is ~0.3. Shown in Fig. 11 is just this case, which shows the central part of the distribution of extremely low divergence; however, the tails are more significant than the $\rho = 0.4$ case. Measured power deposition[146] for multibeamlet systems shows just the kind of behavior shown in Figs. 7–11, with tails significantly larger than Gaussians.[147]

Beam divergence is shown as a function of perveance $\eta\rho$ in Fig. 12. The fraction of beam transmitted compared to that outside the geometric shadow of the plasma electrode is denoted by η. The following three measures of beam divergence are shown: (1)the beam envelope considering 98 initial orbits is denoted by circles, (2) the total rms angle of the transmitted beam is denoted by squares, and (3) the rms angle of the beam, truncated by neglecting the trajectories larger than the total rms average is denoted by triangles. Consistent with Figs. 7–10, the optimum perveance is lowest for the truncated average and higher for the total average and the envelope. This is consistent with measurements of power deposition that have recently been carried out.[146] The truncated average probably closely resembles findings of half-maximum profile measurements[66,67,73] while the total rms angle represents findings of half power through a hole.[146,148]

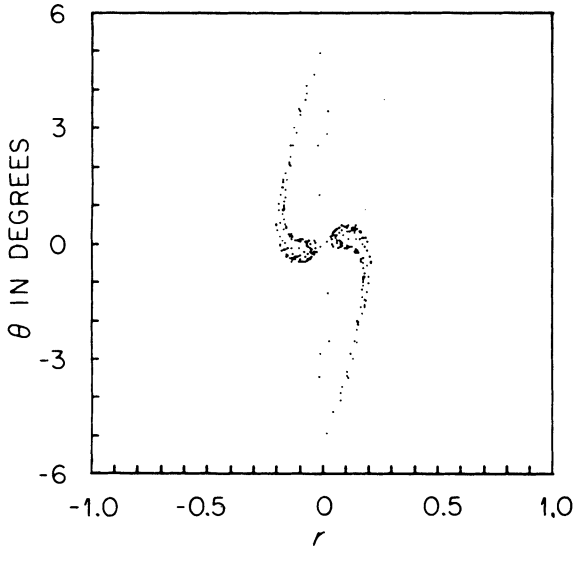

FIGURE 11 Emittance diagram for the case ($\rho = 0.3$) where the beam intensity profile half width is a minimum.

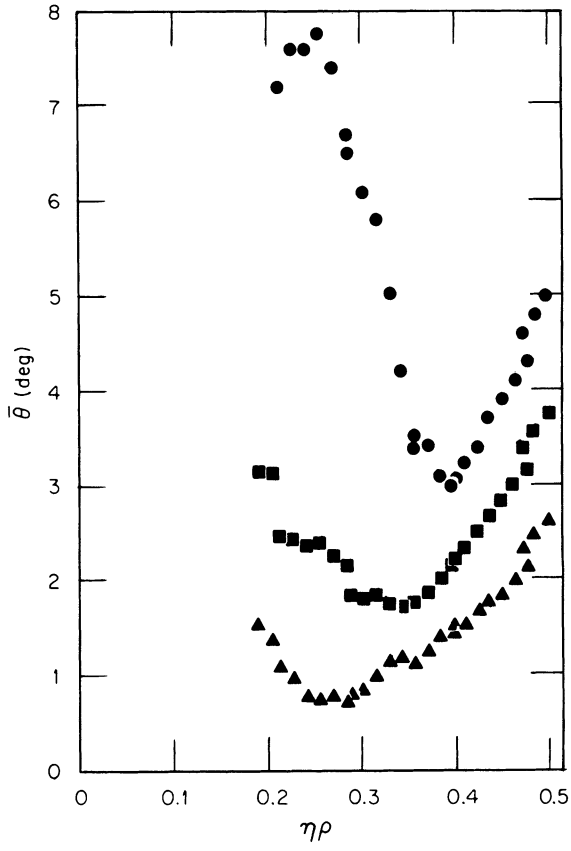

FIGURE 12 Beam divergence as a function of perveance: beam envelope for 98 initial orbits is denoted by circles, rms angle is denoted by squares, and rms angle of a truncated distribution, as described in the text, is shown by the triangles.

B. *Electron Temperature*

Shown in Fig. 13 are trajectory and potential calculations for an electron temperature varying over two orders of magnitude. Even though the sheath thickness varies by over an order of magnitude, the ion optics at the same source plasma density parameter (ρ) is virtually identical. This result was suggested by previous results[64] using

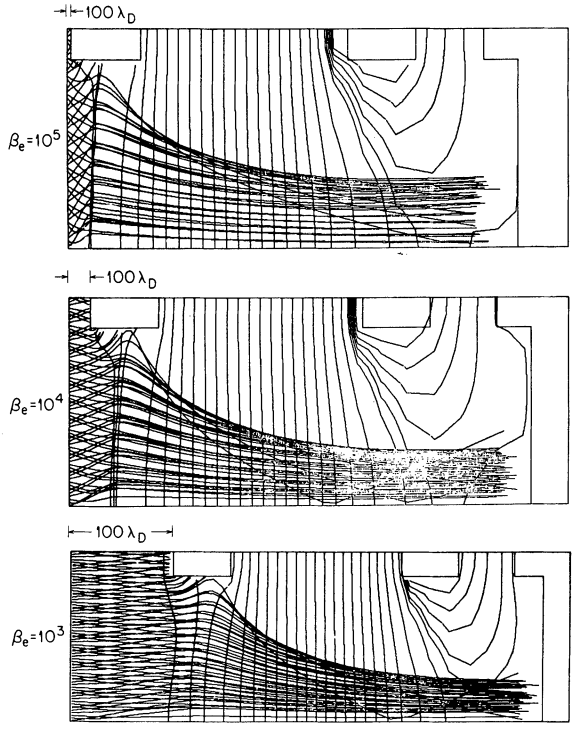

FIGURE 13 Equipotential contours, electrodes, and ion trajectories for three electron temperatures showing the sheath thickness and shape.

a less accurate computational method[68] over a limited range. More detail is shown in the emittance diagrams (Figs. 14–16) for the same cases as shown in Fig. 13(a–c), respectively. Both low (Fig. 14) and high (Fig. 16) electron temperatures show some ripples in the sheath shape compared with the intermediate case (Fig. 15). However, the effect of such ripples on ion optics is on the order of ion thermal effect ($\beta_i = 10^5$) and much smaller than aberration effects. Ion optics is shown in Fig. 17 as a function of electron temperature at optimum perveance showing virtual independence from the electron temperature. Transmission efficiency at optimum perveance ($\eta\rho_{opt}$) and optimum perveance are shown as a function of electron temperature in Fig. 18. The optimum perveance for minimum rms divergence increases for increasing electron temperature.

C. *Plasma Potential*

The plasma potential with respect to the plasma electrode has a considerable effect upon ion optics. Shown in Fig. 19 is the beam rms divergence

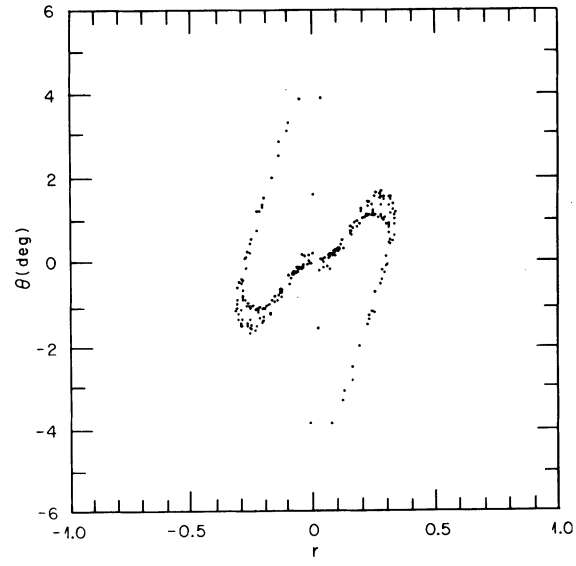

FIGURE 14 Emittance diagram for the case considered in Fig. 13(a).

angle $\bar{\theta}$ at optimum perveance as a function of the plasma potential. A parameter μ is defined as the ratio of the plasma electrode potential to the accelerating potential, both with respect to the plasma potential. For the electron temperature considered, $\beta_e = 3000$, the potential for an isolated plasma electrode[136] is at $\mu = 0.0013$.

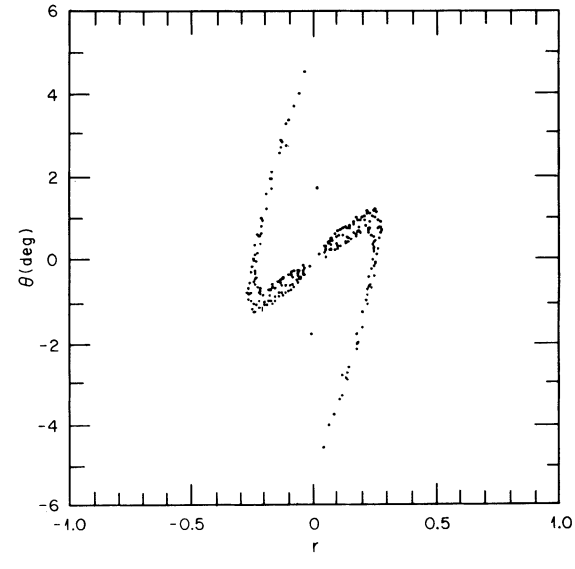

FIGURE 15 Emittance diagram for the case considered in Fig. 13(b).

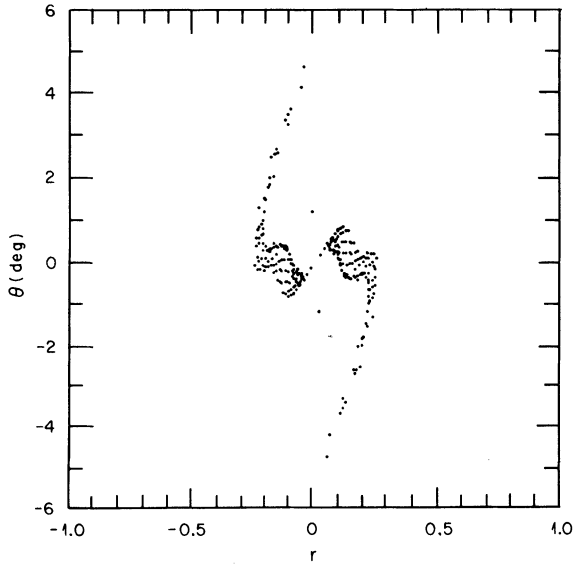

FIGURE 16 Emittance diagram for the case considered in Fig. 13(c).

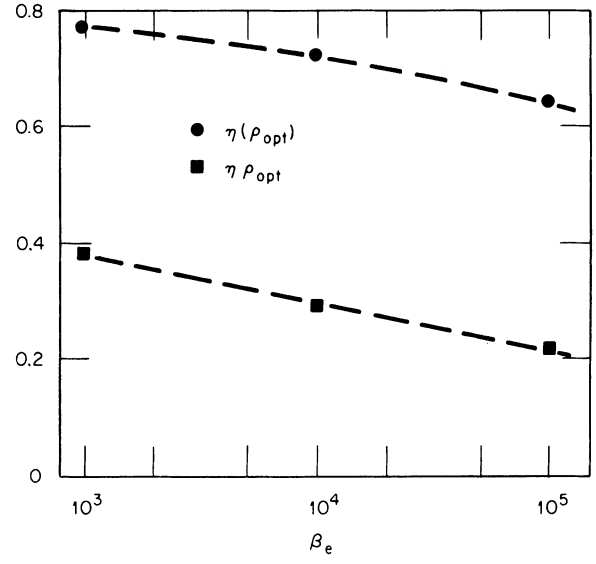

FIGURE 18 Transmission efficiency as a function of electron temperature.

Plasma potential is either significantly higher than this (negative bias) or lower (positive bias), causing lower beam divergence. The oscillations in Fig. 19 are attributed to a finite number of orbits in the solution of the Vlasov equation. The most divergent trajectories for 96 initial orbits as a function of μ are shown in Fig. 20. The perveances are the same as the corresponding ones for the points in Fig. 19. As can be seen from Fig. 20, the wings of the beam distribution also diminish significantly for both positive and negative bias. The optimum perveance for minimum beam divergence as a function of μ is shown in Fig. 21. As a function of μ, the optimum perveance decreases as μ is increased. The fraction of extracted ions to those outside the geometric shadow of the plasma electrode (which are available for extraction) is shown in Fig. 22. In contrast with the usual extraction efficiency of around $\eta = 0.7$, the transmission is 1 for extreme values of biasing and reaches a minimum of

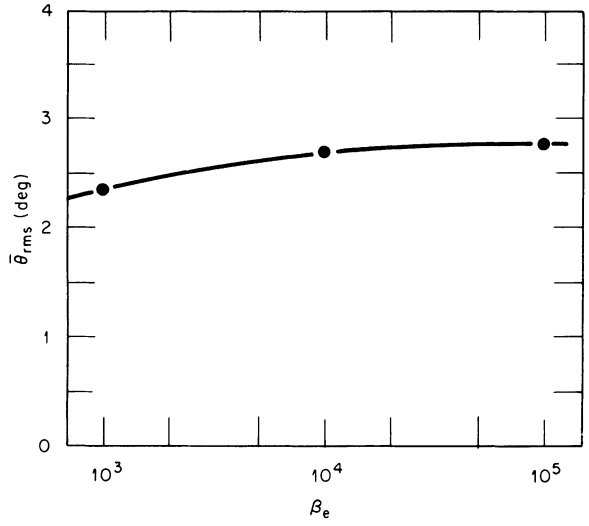

FIGURE 17 Beam divergence as a function of electron temperature.

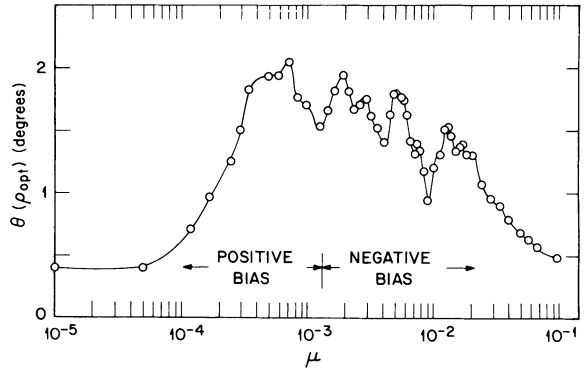

FIGURE 19 Beam rms divergence as a function of plasma potential with respect to the plasma electrode.

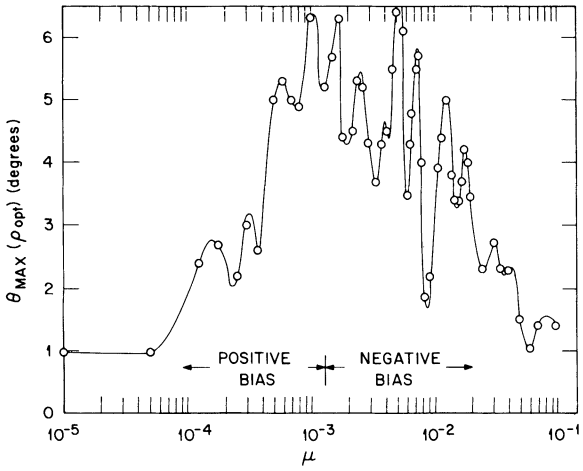

FIGURE 20 Beam envelope as a function of plasma potential with respect to the plasma electrode.

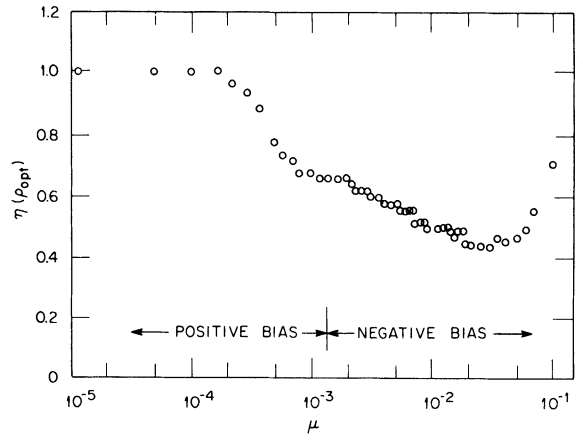

FIGURE 22 Fraction of extracted ions to those outside the geometric shadow of the plasma electrode as a function of plasma potential with respect to the plasma electrode.

~0.42 for a substantial negative bias. Extreme positive bias appears to be a panacea in terms of low divergence and high optimum perveance, but, as shown in Fig. 23, there is a defect. The sensitivity to plasma density variations, denoted by Q,[107] is shown in Fig. 23 as a function of plasma potential. For positive bias the sensitivity becomes extreme and the requirements on source noise and plasma uniformity are extreme.

Figure 24 shows trajectories and equipotential lines for three different values of plasma potential. Figure 25 shows the respective emittance diagrams for these cases. From these figures, one can see many of the mechanisms operating to give less divergence with either positive or negative bias as compared to an isolated plasma electrode. The easiest case to explain is shown in Fig. 24(c); for extreme negative biasing, the ions go through the aberration fields of the plasma electrode with relatively large velocity (compared with the isolated electrode case), so that the dispersion produced by these fields is small. For small negative bias, besides the effect mentioned above, the plasma electrode absorbs more ions than the isolated electrode case. The extra absorbed ions are just the ones that would have been most influenced by the aberration

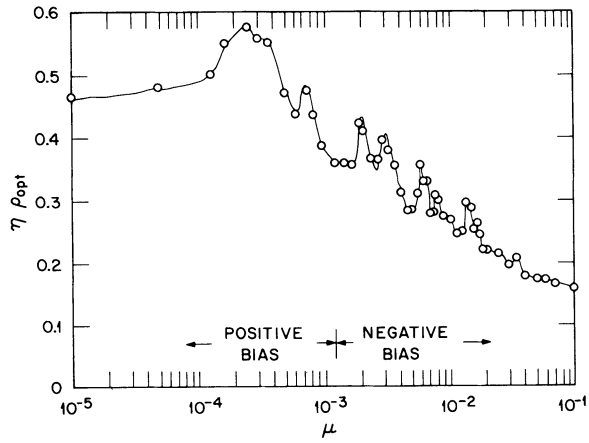

FIGURE 21 Optimum perveance as a function of plasma potential with respect to the plasma electrode.

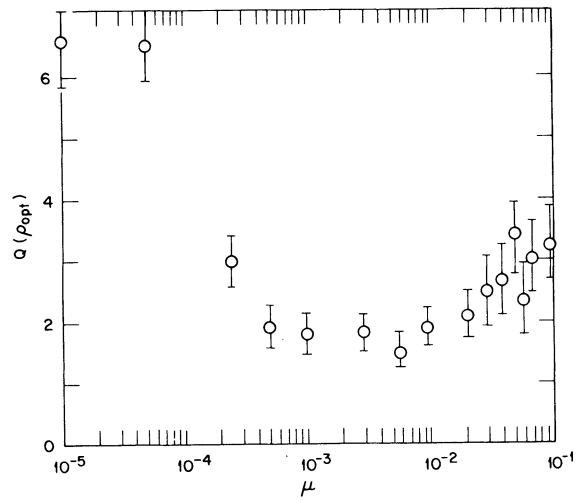

FIGURE 23 Sensitivity of optics to plasma density variations as a function of plasma potential with respect to the plasma electrode.

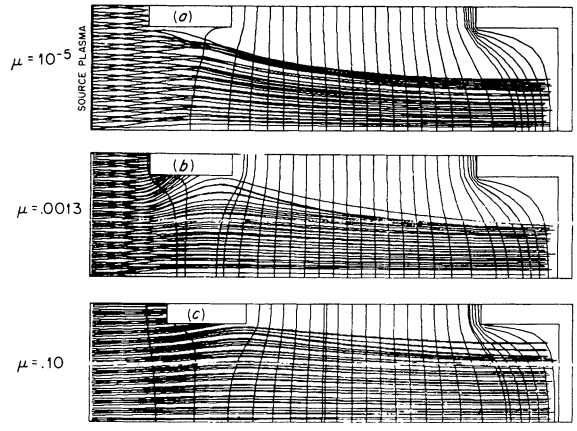

FIGURE 24 Equipotential contours, electrodes, and trajectories for three different source plasma potentials with respect to the plasma electrode.

fields. This effect has been observed experimentally for small negative biasing ($0.002 < \mu < 0.01$).[148] Positive biasing causes the plasma to move into the aperture farther, thus partially cancelling out the aberration fields directly. This cancellation is the same effect produced by the tetrode in some operating regimes.[66]

D. Source Noise

Source noise was previously investigated using this code in the adiabatic approximation, where it was assumed that the plasma ion density fluctuations were slow compared with the relaxation time of the electrons.[107] Principal results are shown in Fig. 26 on the curve labeled A. More results will be described in the next section on the effect of electrode dimensions on ion optics.

IV. EFFECT OF ELECTRODE DIMENSIONS ON ION OPTICS

The effect of electrode shapes similar to those in the illustrative cases considered in the previous section can be deduced from already established similarity principles.[64] Non-similar electrode configurations are considered in this section.

A. Aspect Ratio (variation of electrode radius)

Various radius electrodes are shown in Figs. 27–31. Figure 27 shows orbits and equipotential

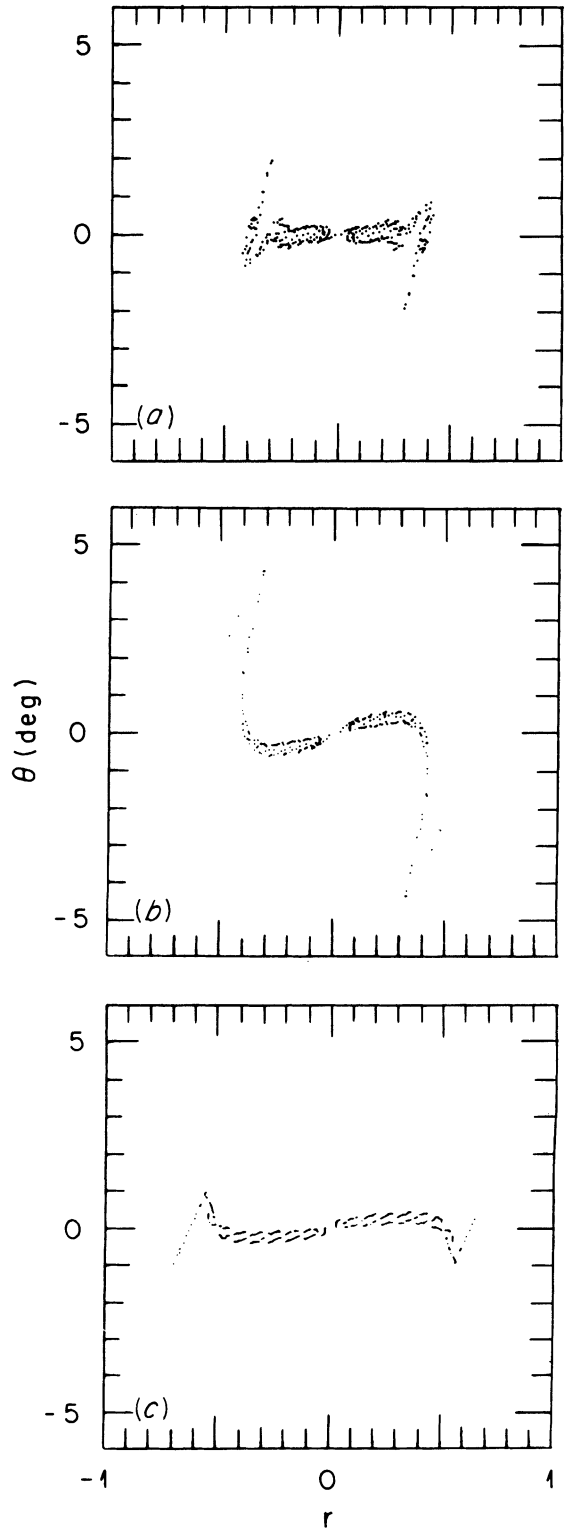

FIGURE 25 Emittance diagram for the three cases considered in Fig. 24.

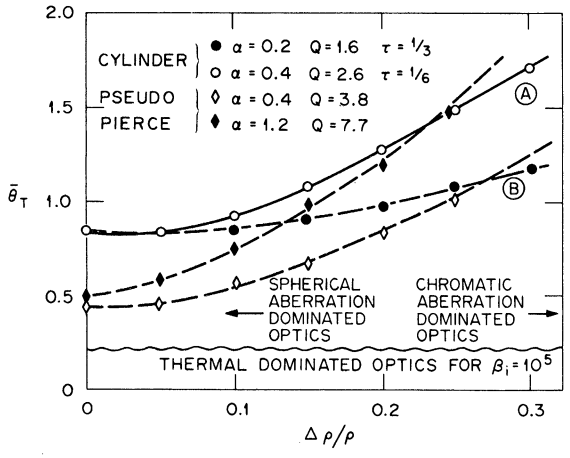

FIGURE 26 Effect of beam optics as a function of source noise for two different plasma electrode shapes and gap distances.

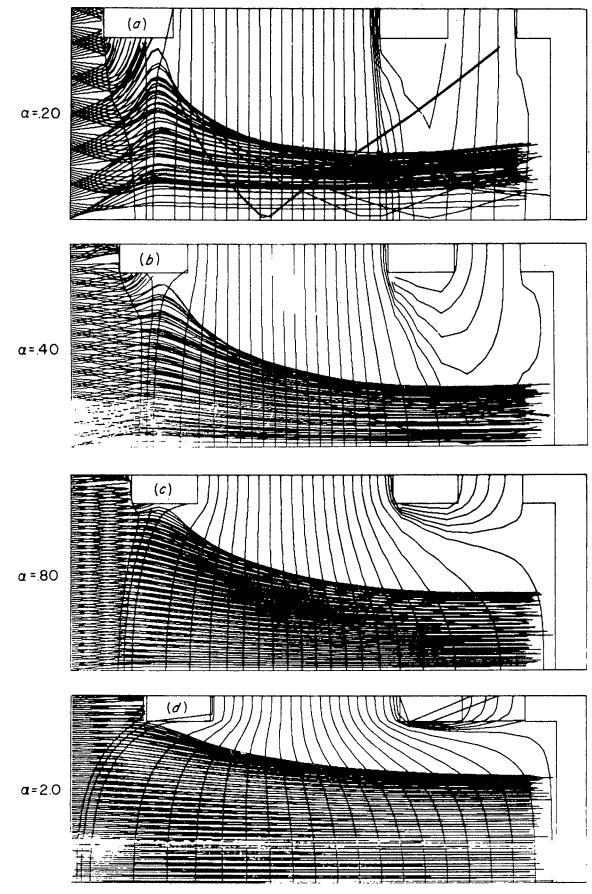

FIGURE 27 Equipotential contours, electrodes, and ion trajectories for four different radius apertures; case C corresponds to the correct scale.

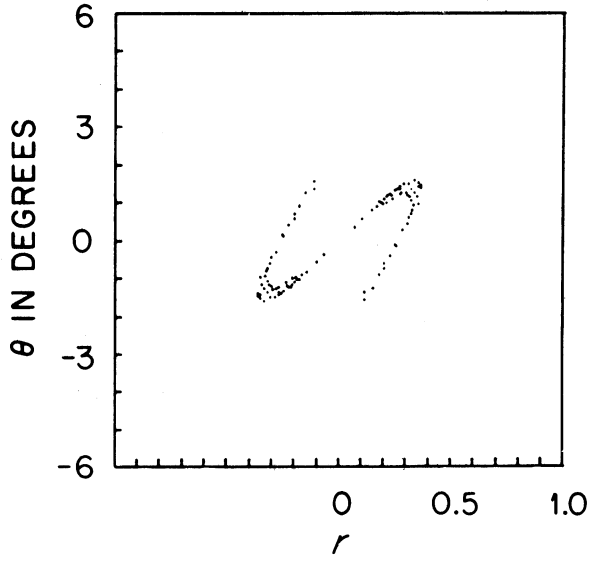

FIGURE 28 Emittance diagram for the case shown in Fig. 27(a).

contours. The radial and longitudinal scales are equal in the case $\alpha = r/d = 0.80$ shown in Figs. 27(c) and 30. In other cases, a radial expansion or compression is shown. Each case shown is almost at optimum perveance for the minimum rms beamlet divergence. However, as can be seen in Fig. 27, the effect of aberrations is dif-

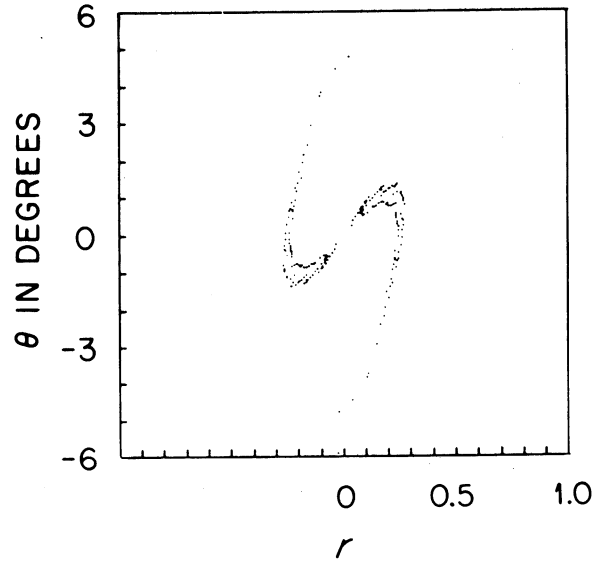

FIGURE 29 Emittance diagram for the case shown in Fig. 27(b).

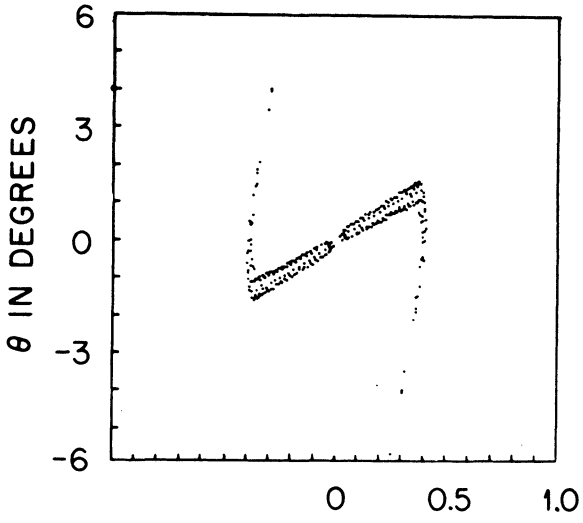

FIGURE 30 Emittance diagram for the case shown in Fig. 27(c).

ferent. The aberrations for the large-radii case [Figs. 27(d) and 31] have weaker aberrations than the smaller-radii case [Figs. 27(a) and 28], but these weaker aberrations affect a larger fraction of the ions that traverse the accelerator. These two effects apparently cancel to first order, be-

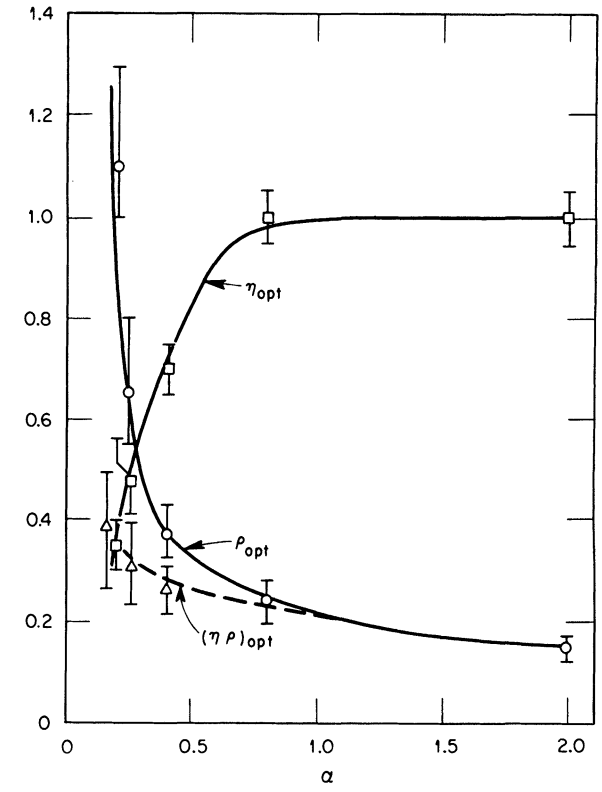

FIGURE 32 Optimum perveance and a transmitted fraction as a function of aspect ratio.

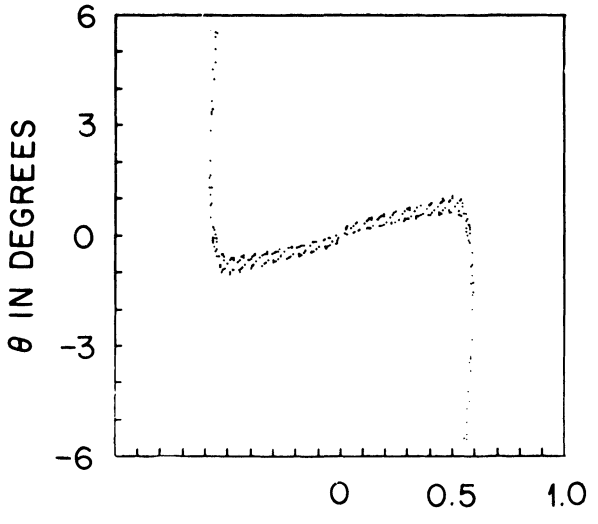

FIGURE 31 Emittance diagram for the case shown in Fig. 27(d).

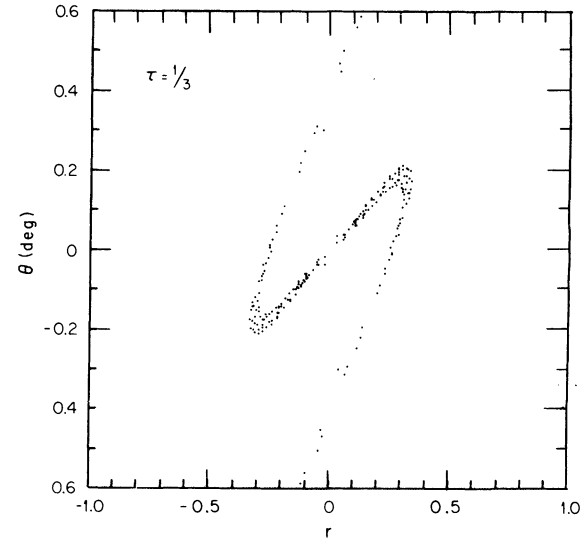

FIGURE 33 Emittance diagram for a thin ($\tau = 1/15$) plasma electrode near optimum perveance, showing relatively small aberrations.

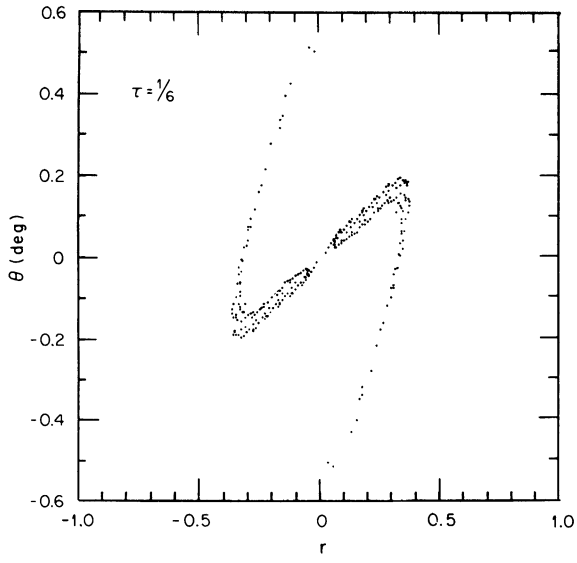

FIGURE 34 Emittance diagram for a thicker (τ = 1/6) plasma electrode near optimum perveance.

cause the beamlet divergence is found to be independent of electrode radius. Plasma-electrode absorption of ions is more dominant for the small-radius case [Figs. 27(a) and 28]. Field penetration is greater for the large-aperture case, which causes a lower optimum perveance for minimum beamlet divergence. These latter two effects are shown quantitatively in Fig. 32, in which optimum perveance and transmitted fraction at optimum perveance are plotted as functions of aspect ratio. The optimum plasma density parameter ρ_{opt} is also shown. These results show that for large radius, virtually no ions outside the geometric shadow of the plasma electrode are lost to the electrode. The requirement of plasma density for optimum perveance is very severe for small-radii electrodes. We have neglected to verify the decelerating potential (as a function of electrode radius) that will be necessary to block electrons at the larger radii. For those radii above α = 0.40, this decelerating potential will have to be increased.

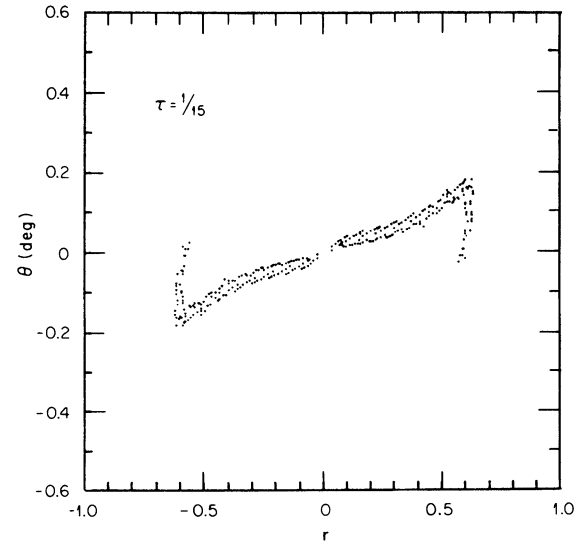

FIGURE 35 Emittance diagram for a thicker (τ = 1/3) plasma electrode near optimum perveance, showing dominance of aberrations.

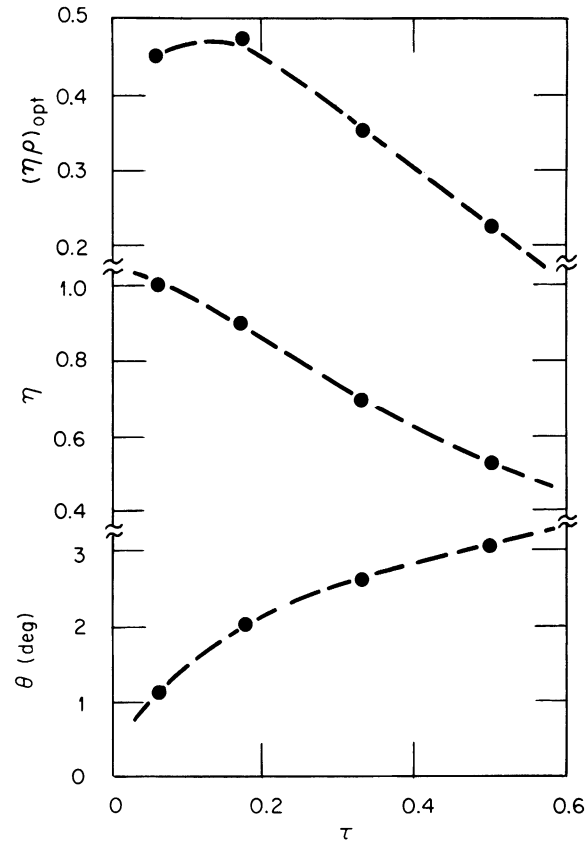

FIGURE 36 Optimum perveance, transmitted fraction, and beam divergence as a function of plasma electrode thickness.

B. *Thickness of Electrodes*

Variation in ion optics as a function of electrode thickness is shown in the emittance diagrams of Figs. 33–35; the thickness parameter is the electrode thickness divided by the accelerating gap.

As the thickness of the electrodes diminishes, the aberrations decrease. Additional information is shown in Fig. 36. In particular, for thick electrodes the fraction of ions transmitted outside the geometric shadow of the electrodes diminishes significantly. This is reflected in a decrease of the optimum perveance, not because the sheath is farther back, as in the situation shown in Fig. 32, but because there is a dearth of ions in the sheath due to its diminished cross-sectional area. From the foregoing we see that thick electrodes have a triply degenerate effect: the beam divergence is increased, the current density that can be extracted is less, and the required plasma density is slightly higher. These results can be used in combination with those of the previous section to deduce the optics and properties of single-stage accelerators over a wide variety of physical parameters. A special property of elongated accelerators (large gap compared with radius) is shown in Fig. 26 for the cases denoted by the curves labeled A (short) and B (long), namely, that the sensitivity to source plasma noise or density inhomogeneities is significantly reduced.

V. CONCLUSIONS

Inclusion of plasma electrons with an absolutely converging nonlinear scheme is necessary for a reliable solution for the optics of ions extracted through apertures. Algorithms without explicit inclusion of plasma electrons have a dubious foundation because the sheath for a non-Pierce geometry, even in the $T_e \rightarrow 0$ limit, does not approach the surface presumed. Algorithms that explicitly include plasma electrons, but which do not have a wide radius of convergence, usually demand that the starting point for the orbits be in the sheath itself as opposed to substantially before the sheath. Such a boundary condition requires a stipulation of the sheath properties on a two-dimensional surface; because only a one-dimensional analysis has been done for this situation, this stipulation is not without difficulty. For example, the magnitude of the electric field on an equipotential corresponding to the classical sheath edge is not constant over the surface, as is usually presumed for algorithms that start there.

A principal disadvantage of the algorithm described here is the fluctuations which appear for small changes of a parameter.

Principle *a priori* predictions of this algorithm for reducing beamlet divergence are applications of a negative bias to the first (or plasma) electrode (verified experimentally) and a small positive bias, relative to its potential under isolation (not yet examined experimentally).

ACKNOWLEDGMENTS

We wish to thank E. F. Jaeger, L. D. Stewart, W. L. Stirling, C. C. Tsai, L. R. Grisham, and R. W. McGaffey for their help.

This research was sponsored by the Office of Fusion Energy, U.S. Department of Energy under contract W-7405-eng-26 with the Union Carbide Corporation.

REFERENCES

1. J. M. Dawson, H. P. Furth, and F. H. Tenney, *Phys. Rev. Lett.* **26,** 1156 (1971).
2. T. H. Stix, *Plasma Phys.* **14,** 367 (1972).
3. G. G. Kelley et al., *Nucl. Fusion* **12,** 169 (1972).
4. J. P. Girard, M. Khelladi, and D. A. Marty, *Nucl. Fusion* **13,** 685 (1973).
5. D. R. Sweetman, *Nucl. Fusion* **13,** 157 (1973).
6. J. A. Rome, J. D. Callen, and J. F. Clarke, *Nucl. Fusion* **14,** 141 (1974).
7. J. G. Cordey and W. G. F. Core, *Phys. Fluids* **17,** 1626 (1974).
8. K. Bol et al., *Phys. Rev. Lett.* **32,** 661 (1974).
9. J. Jacquinot et al., *Nucl. Fusion* **15,** 3 (1975).
10. R. Bir et al., *Nucl. Fusion* **15,** 17 (1975).
11. J. G. Cordey and W. G. F. Core, *Nucl. Fusion* **15,** 710 (1975).
12. L. A. Berry et al., *Phys. Rev. Lett.* **34,** 1085 (1975).
13. J. A. Rome et al., *Nucl. Fusion* **16,** 55 (1976).
14. J. D. Callen, *Comments on Plasma Phys. and Controlled Fusion* **2,** 159 (1976).
15. D. L. Jassby, *Nucl. Fusion* **17,** 309 (1977).
16. O. B. Morgan, G. G. Kelley, and R. C. Davis, *Rev. Sci. Instrum.* **4,** 467 (1967).
17. G. W. Hamilton, J. L. Hilton, and J. S. Luce, *Plasma Phys.* **10,** 687 (1968).
18. R. C. Davis, O. B. Morgan, L. D. Stewart, and W. L. Stirling, *Rev. Sci. Instrum.* **43,** 278 (1972).
19. W. S. Cooper, K. H. Berkner, and R. V. Pyle, *Nucl. Fusion* **12,** 263 (1972).
20. K. W. Ehlers et al., *J. Vac. Sci. Technol.* **10,** 922 (1973).
21. D. Aldcroft et al., *Nucl. Fusion* **13,** 393 (1973).
22. M. Fumelli, *Nucl. Instrum. Methods* **118,** 337 (1974).
23. R. C. Davis et al., *Rev. Sci. Instrum.* **46,** 576 (1975).
24. M. Fumelli and F. P. G. Valckx, *Nucl. Instrum. Methods* **135,** 203 (1976).
25. W. L. Stirling, C. C. Tsai, and P. M. Ryan, *Rev. Sci. Instrum.* **48,** 533 (1977).
26. D. M. Goebel, J. T. Crow, and A. T. Forrester, *Rev. Sci. Instrum.* **49,** 469 (1978).

27. K. N. Leung et al., *Rev. Sci. Instrum.* **49,** 321 (1978).
28. W. L. Stirling et al., *Rev. Sci. Instrum.* **50,** 102 (1979).
29. C. E. S. Phillips, *Proc. R. Soc.* (London) **A64,** 174 (1898).
30. C. E. S. Phillips, Philos. *Trans. R. Soc.* (London) **A197,** 135 (1901).
31. R. J. Strutt, *Proc. R. Soc.* (London) **A89,** 68 (1913).
32. M. Wehrli, *Ann. Physik* **69,** 285 (1922).
33. F. M. Penning, *Physica* (Utrecht) **4,** 71 (1937).
34. F. M. Penning and J. H. A. Moubis, *Physica* (Utrecht) **4,** 1190 (1937).
35. E. B. Hooper, *Adv. Electron. Electron Phys.* **27,** 295 (1969).
36. C. C. Tsai, W. L. Stirling, and P. M. Ryan, *Rev. Sci. Instrum.* **48,** 651 (1977).
37. P. M. Ryan et al., *Bull. Am. Phys. Soc.* **20,** 1365 (1975); L. D. Stewart et al., *Bull. Am. Phys. Soc.* **19,** 912 (1974); T. C. Jernigan et al., *Bull. Am. Phys. Soc.* **17,** 974 (1972); O. B. Morgan, *Bull. Am. Phys. Soc.* **17,** 974 (1972).
38. S. Matsuda et al., *Bull. Am. Phys. Soc.* **18,** 132 (1973).
39. TFR Group, Fontenay-aux-Roses Report EUR-CEA-FC-834, 1976 (unpublished).
40. S. Matsuda et al., Japan Atomic Energy Research Institute Report JAERI-M 6431, Tokai, Japan, 1976 (unpublished); English translation available as ORNL-Tr-4168 (Oak Ridge, TN).
41. Y. Ohara et al., *7th IEEE Symp. on Eng. Prob. in Fusion Research* (Knoxville, TN, 1977).
42. J. H. Feist et al., *IEEE 7th Symp. on Eng. Prob. in Fusion Research* (Knoxville, TN, 1977).
43. T. Sugawara et al., Japan Atomic Energy Research Institute Report JAERI-M-7043, Tokai, Japan, 1977 (unpublished).
44. T. L. Churchill, *IEEE Conf. on Plasma Science*, Troy, NY, 1977 (unpublished).
45. M. Fumelli and R. Becherer, Fontenay-aux-Roses Laboratory Report #EUR-CEA-FC-901, Fontenay-aux-Roses, France, 1977 (unpublished).
46. R. Becherer, M. Fumelli and F. R. G. Valckx, *IEEE 7th Symp. on Eng. Prob. in Fusion Research* (Knoxville, TN, 1977).
47. K. W. Ehlers and W. B. Kunkel, *Proc. 2nd Conf. on Ion Sources*, Vienna, Austria, 1972 (unpublished).
48. K. W. Ehlers et al., *Bull. Am. Phys. Soc.* **17,** 973 (1972); K. H. Berkner et al., *Bull. Am. Phys. Soc.* **17,** 973 (1972).
49. K. W. Ehlers et al., *Bull. Am. Phys. Soc.* **19,** 895 (1974); K. H. Berkner et al., *Bull. Am. Phys. Soc.* **19,** 895 (1974).
50. K. H. Berkner et al., *2nd Symp, on Ion Sources and Formation of Ion Beams,* Berkeley, CA, 1974 (unpublished).
51. V. M. Kulygin et al., *2nd Symp. on Ion Sources and Formation of Ion Beams,* Berkeley, CA, 1974 (unpublished).
52. S. M. Hibbs, *IEEE 6th Symp. on Eng. Prob. in Fusion Research,* San Diego, CA, 1975 (unpublished).
53. K. W. Ehlers et al., *9th Symp. Fusion Tech.,* Garmisch, Germany, 1976 (unpublished).
54. K. H. Berkner et al., *Bull. Am. Phys. Soc.* **21,** 1136 (1976).
55. K. W. Ehlers, *IEEE Conf. on Plasma Science,* Troy, NY, 1977 (unpublished); K. H. Berkner, *ibid.*
56. K. H. Berkner et al., *Bull. Am. Phys. Soc.* **22,** 1082 (1977); also in *IEEE 7th Symp. on Eng. Prob. in Fusion Research,* Knoxville, TN, 1977 (unpublished); K. W. Ehlers, *ibid.*
57. V. V. Fosnight, T. R. Dillon, and G. Sohl, *J. Spacecraft* **7,** 226 (1970).
58. L. D. Stewart, J. Kim, and S. Matsuda, *Rev. Sci. Instrum.* **46,** 1193 (1975).
59. J. R. Coupland and T. S. Green, *Nucl. Instrum. Methods* **125,** 197 (1975).
60. T. Sagawara and Y. Ohara, *Japan J. Appl. Phys.* **14,** 1029 (1975).
61. H. H. Haselton et al., *IEEE 6th Symp. on Eng. Prob. in Fusion Research,* San Diego, CA, 1975 (unpublished).
62. J. Kim and R. C. Davis, *Appl. Phys. Lett.* **20,** 130 (1977).
63. N. Sakudo, K. Tokiguchi, H. Koike, and I. Kanonmata, *Rev. Sci. Instrum.* **48,** 762 (1977).
64. J. H. Whealton, E. F. Jaeger, and J. C. Whitson, *Rev. Sci. Instrum.* **48,** 829 (1977).
65. J. H. Whealton, *Rev. Sci. Instrum.* **48,** 1428 (1977).
66. J. Kim, J. H. Whealton, and G. Schilling, *J. Appl. Phys.* **49,** 517 (1978).
67. J. H. Whealton et al., *J. Appl. Phys.* **49,** 3091 (1978).
68. J. H. Whealton, E. F. Jaeger, and J. C. Whitson, *J. Comput. Phys.* **27,** 32 (1978).
69. J. C. Whitson, J. Smith, and J. H. Whealton, *J. Comput. Phys.* **28,** 408 (1978).
70. E. Thompson, *Particle Accelerators* **4,** 69 (1972).
71. J. R. Coupland et al., *Rev. Sci. Instrum.* **44,** 1258 (1973).
72. T. S. Green, *J. Appl. Phys.* **D9,** 1165 (1976).
73. L. R. Grisham et al., *Rev. Sci. Instrum.* **48,** 1037 (1977).
74. H. R. Kaufman, *Adv. in Electron. Electron Phys.* **36** (1974).
75. T. S. Green, *Rep. Prog. Phys.* **37,** 1257 (1974).
76. T. S. Green, *IEEE Trans. Nucl. Sci.* **NS23,** 918 (1976).
77. Y. Ohara et al., *Japan J. Appl. Phys.* **15,** 135 (1976).
78. G. Sohl and V. V. Fosnight, *J. Spacecraft* **6,** 143 (1969).
79. R. L. Seliger et al., *J. Spacecraft* **7,** 422 (1970).
80. G. R. Nudd and K. Amboss, *AIAA J.* **8,** 649 (1970).
81. Y. Ohara, Japan Atomic Energy Research Institute Report JAERI-M-6813, Tokai, Japan, 1976 (unpublished).
82. H. R. Kaufman, Lewis Research Center Report TND-585, NASA, Cleveland, 1961 (unpublished).
83. W. C. Lathem, *J. Spacecraft* **5,** 735 (1968).
84. X. P. Grigorev, *Sov. Phys.-Tech. Phys.* **16,** 909 (1971).
85. K. Asai et al., *Japan J. Appl. Phys.* **15,** 1343 (1976).
86. W. S. Cooper, K. Halbach, and S. B. Majyary, *2nd Symp. on Ion Source Formation of Beams,* Berkeley, CA, 1974 (unpublished).
87. E. Thompson, *2nd Symp. on Ion Sources,* Berkeley, CA, 1974 (unpublished).
88. C. D. Child, *Phys. Rev.* **32,** 492 (1911).
89. I. Langmuir, *Phys. Rev.* **2,** 450 (1913).
90. I. Langmuir and K. R. Blodgett, *Phys. Rev.* **24,** 49 (1924).
91. C. J. Davisson and C. J. Calbick, *Phys. Rev.* **38,** 585 (1931).
92. C. J. Davisson and C. J. Calbick, *Phys. Rev.* **42,** 580 (1932).
93. E. E. Watson, *Philos. Mag.* **3,** 849 (1927).
94. B. Van Barries and J. Dosse, *Arch. Elektrotech.* (Berlin) **32,** 221 (1938).
95. B. J. Thompson and L. B. Headrich, *Proc. Institute of Radio Engineer.* **28,** 318 (1940).
96. H. Moss, *Wireless Eng.* **22,** 316 (1945).
97. J. R. Pierce, *Theory and Design of Electron Beams* (Van Nostrand, New York, 1954).
98. C. D. Moak, *Nucl. Instrum. Methods* **8,** 19 (1960).
99. B. S. Kuznetsov, *Radiotekh. Elektron.* **8,** 1385 (1962).

100. P. T. Kirstin, G. S. Kino, and W. E. Waters, *Space Charge Flow* (McGraw Hill, New York, 1967).
101. E. Hara, *Nucl. Instrum. Methods* **63,** 313 (1968).
102. G. Bosi, *J. Appl. Phys.* **44,** 2188 (1973).
103. G. Bosi, *J. Appl. Phys.* **46,** 4689 (1975).
104. T. S. Green, *J. Phys.* **D9,** 1165 (1976).
105. G. Bosi, *J. Appl. Phys.* **47,** 5292 (1976).
106. J. H. Whealton, *Appl. Phys. Lett.* **32,** 353 (1978).
107. J. H. Whealton and C. C. Tsai, *Rev. Sci. Instrum.* **49,** 495 (1978).
108. E. R. Harrison, *J. Appl. Phys.* **29,** 909 (1958).
109. G. G. Kelley, N. H. Lazar, and O. B. Morgan, *Nucl. Instrum. Methods* **10,** 263 (1961).
110. J. Kistemaker, *Nucl. Instrum. Methods* **11,** 179 (1961).
111. J. Hyman et al., *AIAA J.* **2,** 1739 (1964).
112. N. B. Brooks et al., *Rev. Sci. Instrum.* **35,** 894 (1964).
113. O. B. Morgan, G. G. Kelley, and R. C. Davis, *Rev. Sci. Instrum.* **38,** 467 (1967).
114. N. K. Majumdar, *Nucl. Instrum. Methods* **88,** 205 (1970).
115. J. R. Coupland and E. Thompson, *Rev. Sci. Instrum.* **42,** 1034 (1971).
116. T. Sugawara and Y. Ohara, *Japan J. Appl. Phys.* **14,** 1029 (1975).
117. Y. Ohara, Japan Atomic Energy Research Institute Report M6813, Tokai, Japan, 1976 (unpublished).
118. M. D. Gabovich, *Instrum. Exp. Tech.* **2,** 195 (1963).
119. D. G. Bate, Culham Laboratories Report CLM R53, 1966 (unpublished).
120. V. Hamza and E. A. Richley, Lewis Research Center Report TND-1323, NASA, Cleveland, 1962 (unpublished).
121. V. Hamza and E. A. Richley, Lewis Research Center Report TND-1665, NASA, Cleveland, 1963 (unpublished).
122. P. T. Kirstein and J. S. Hornsby, Geneva Report CERN 63-16, Geneva, 1963 (unpublished).
123. V. Hamza, Lewis Research Center Report TND-1711, NASA, Cleveland, 1963 (unpublished).
124. P. T. Kirstein and J. S. Hornsby, *IEEE Trans. Electron Devices* **11,** 196 (1964).
125. C. D. Bogart and E. A. Richley, Lewis Research Center Report TND-3394, NASA, Cleveland, 1966 (unpublished).
126. J. L. Harrison, *J. Appl. Phys.* **39,** 3827 (1968).
127. G. R. Nudd and K. Amboss, *AIAA J.* **8,** 649 (1970).
128. B. I. Valkov, A. G. Sveshnikov, and N. N. Semashko, *Sov. Phys.-Dokl.* **16,** 1040 (1972).
129. V. S. Boldasov et al., *Sov. Phys. -Dokl.* **19,** 652 (1975).
130. W. W. Hicks et al., *Nucl. Instrum. Methods* **139,** 25 (1976).
131. Y. Ohara et al., *Japan J. Appl. Phys.* **17,** 423 (1978).
132. H. R. Kaufman, *AIAA J.* **15,** 1025 (1977).
133. Y. Ohara, *J. Appl. Phys.* **49,** 4711 (1978).
134. K. Halbach, Lawrence Berkeley Laboratory Report LBL-4444, Berkeley, CA, 1975 (unpublished).
135. E. F. Jaeger and J. C. Whitson, ORNL/TM-4990, Oak Ridge, TN, 1975 (unpublished).
136. S. A. Self, *Phys. Fluids* **6,** 1762 (1963).
137. B. M. Marder, Sandia Report SAND 77-0048, Albuquerque, NM, 1977 (unpublished).
138. J. C. Whitson, E. F. Jaeger, and J. H. Whealton, *Bull. Am. Phys. Soc.* **22,** 1114 (1977).
139. J. C. Whitson et al., ORNL/TM-6512, Oak Ridge, TN (1978).
140. L. J. Drooks et al., *Bull. Am. Phys. Soc.* **23,** 846 (1978).
141. J. M. Ortega and W. C. Rheinboldt, *Iterative Solution of Nonlinear Equations in Several Variables* (Academic Press, New York, 1970).
142. J. H. Hornsby, Geneva Report CERN 63-7, 1963 (unpublished).
143. R. Bulirsch and J. Stoer, *Numer. Math.* **8,** 1 (1966).
144. E. Buckingham, *Phys. Rev.* **4,** 345 (1914).
145. P. W. Bridgeman, *Dimensional Analysis,* 2nd edition (Yale University Press, New Haven, 1931).
146. M. M. Menon et al., *J. Appl. Phys.* **50,** 2484 (1979).
147. J. H. Whealton, ORNL/TM-6421, Oak Ridge, TN (1979).
148. J. H. Whealton et al., *Appl. Phys. Lett.* **33,** 278 (1978).